The impact of small motion on the visualization of coronary vessels and lesions in cardiac CT: A simulation study

Francisco Contijoch[a)]
Department of Medicine, Division of Cardiology, UC San Diego School of Medicine, La Jolla, CA 92123, USA

J. Webster Stayman
Department of Biomedical Engineering, Johns Hopkins University, Baltimore, MD 21218, USA

Elliot R. McVeigh
Department of Bioengineering, UC San Diego School of Engineering, La Jolla, CA 92037-0412, USA
Department of Medicine, Division of Cardiology, UC San Diego School of Medicine, La Jolla, CA 92123, USA
Department of Radiology, UC San Diego School of Medicine, La Jolla, CA 92123, USA

(Received 20 June 2016; revised 27 February 2017; accepted for publication 16 April 2017; published 26 May 2017)

Purpose: Coronary x-ray computed tomography angiography (CCTA) is used to non-invasively assess coronary artery geometry and has, combined with computational modeling, demonstrated the potential to identify physiologically significant lesions. These measurements require robust and accurate coronary imaging and delineation of vessels despite the presence of small motion. This simulation study characterizes the impact of small, uncorrected vessel drifts during data acquisition on the assessment of vessel intensity, diameter, and shape.

Methods: We developed a digital phantom and simulated projection data for a clinical scanner geometry for a range of vessel drifts that can occur during relative vessel stasis (0 to 2 mm per 360° gantry rotation) for vessels between 0.2 and 3.0 mm in diameter (covering 0% through 93% stenosis of a 3 mm vessel). In addition to the impact of vessel drift, we evaluated the performance of half-scan acquisitions (relative to full-scans) over a range of gantry positions. The performance of FDK reconstructions was compared to an iterative technique and potential improvement in sampling from focal spot deflection and quarter detector offset was compared.

Results: At rest, vessel intensity and diameter were accurately obtained in vessels greater than 1.5 mm with all vessels appearing circular in shape (major-to-minor axis ratio ~1). Vessels between 1.5 and 0.2 mm in diameter demonstrated a rapid decrease in signal intensity with full width half maximum (FWHM) vessel diameters remaining above 0.75 mm as true vessel diameter decreased. Uncorrected vessel motion resulted in decreased vessel intensity, increased vessel diameter, and distortion of vessel shape. The extent of these changes depended on both the position of the gantry as well as the reconstruction approach (half- vs. full-scan). FDK reconstruction results depended on choice of filter with Ram-Lak results yielding comparable performance to an unconstrained iterative reconstruction. Focal spot deflection and quarter detector offset did not result in large changes in performance, likely due to the high sampling density near the isocenter.

Conclusions: Despite improvement in gantry speed and acquisition of coronary images during cardiac phases that have relatively stationary vessels, small coronary drifts (0–2 mm per 360° rotation) have been reported and if uncorrected, can present challenges to visual grading and computational modeling of stenoses because vessels will appear dimmer, larger, and more ellipsoidal in shape. The impact of a particular motion depends on the gantry position, the use of half vs. full-scan acquisitions, and the reconstruction technique. © *2017 American Association of Physicists in Medicine* [https://doi.org/10.1002/mp.12295]

Key words: coronary CT angiography, coronary stenosis quantitation, vessel motion

1. INTRODUCTION

In numerous prospective clinical trials, coronary x-ray computed tomography angiography (CCTA) with ≥ 64-slice scanners has demonstrated an excellent ability to rule out obstructive coronary artery disease with extremely high negative predictive value.[1,2] In addition, CCTA "markedly clarifies" the diagnosis of angina due to coronary heart disease and reduces the need for further stress testing,[3] and reduces patient time in the emergency department.[4,5] Furthermore, CT-derived Calcium Scores have proven far superior to all other biomarkers for predicting future major cardiac events.[6]

CCTA has a much higher *sensitivity* for the detection of coronary lesions than existing standard diagnostic techniques.[7] However, the current weakness of CCTA is the frequency of false positive diagnoses of significant coronary disease which reduces its *specificity.* Incorrectly identifying a lesion can lead to unnecessary invasive diagnostic coronary angiograms which do not result in treatment with

percutaneous intervention. This paper explores selected technical reasons why misclassification of lesions may occur.

Lesions are commonly classified on CCTA images by comparing the caliber of the lesion lumen to the caliber of the normal vessel lumen just proximal or distal to the lesion. The recommended approach is to estimate the severity of vessel stenosis as mild (0–50%), moderate (50–70%), or severe (> 70%) based on visual appearance.[8,9] Absolute quantitation of lesion diameter is challenging because the vessel lumen of moderate and severe lesions often falls below 1.5 mm and approaches the limit of the scanner resolution. Quantitation can also be limited by vessels which never come to complete rest during the heart cycle. In fact, the average velocity of the proximal coronary vessels during diastasis is ~10 mm/s[10,11] which means the vessels can move ~2.5 mm during a 250 ms gantry rotation. In this paper, we explore the effects of both the scanner geometry and small vessel drift on lesion characterization.

Although, skilled interpreters of CCTA can very often accurately classify lesions using visual observation, the method would benefit from an objective quantitative approach. Furthermore, new quantitative techniques such as FFR_{CT}[12,13] or plaque characterization[14] require quantitative estimates of lesion geometry and the largest source of uncertainty in the FFR_{CT} estimates arise due to uncertainty in the vessel geometry.[15]

Given the exceptional clinical promise of CCTA, vendors have recently produced a new generation of scanners with wider detectors or dual-source configurations capable of obtaining superb coronary images in a very short time (~66–135 ms).[16–18] This has made a significant impact on both the total dose required and the ability to obtain a diagnostic study in patients with higher heartrates.[19] Even with these new scanners, motion during the acquisition remains an issue forcing vendors to use reduced view reconstructions ("half scan mode") and implement post processing motion correction such as Snapshot Freeze.[20,21] These techniques reduce the number of "unreadable" cases and can improve quantitation of vessel geometry,[22] making CCTA even more powerful for ruling out coronary disease. However, it remains unclear if these techniques can address small coronary vessel drifts during diastasis and what the quantitative impact is of residual motion that remains after motion correction.

This work is motivated by clinical findings shown in Fig. 1 where the observed intensity and diameter of a left

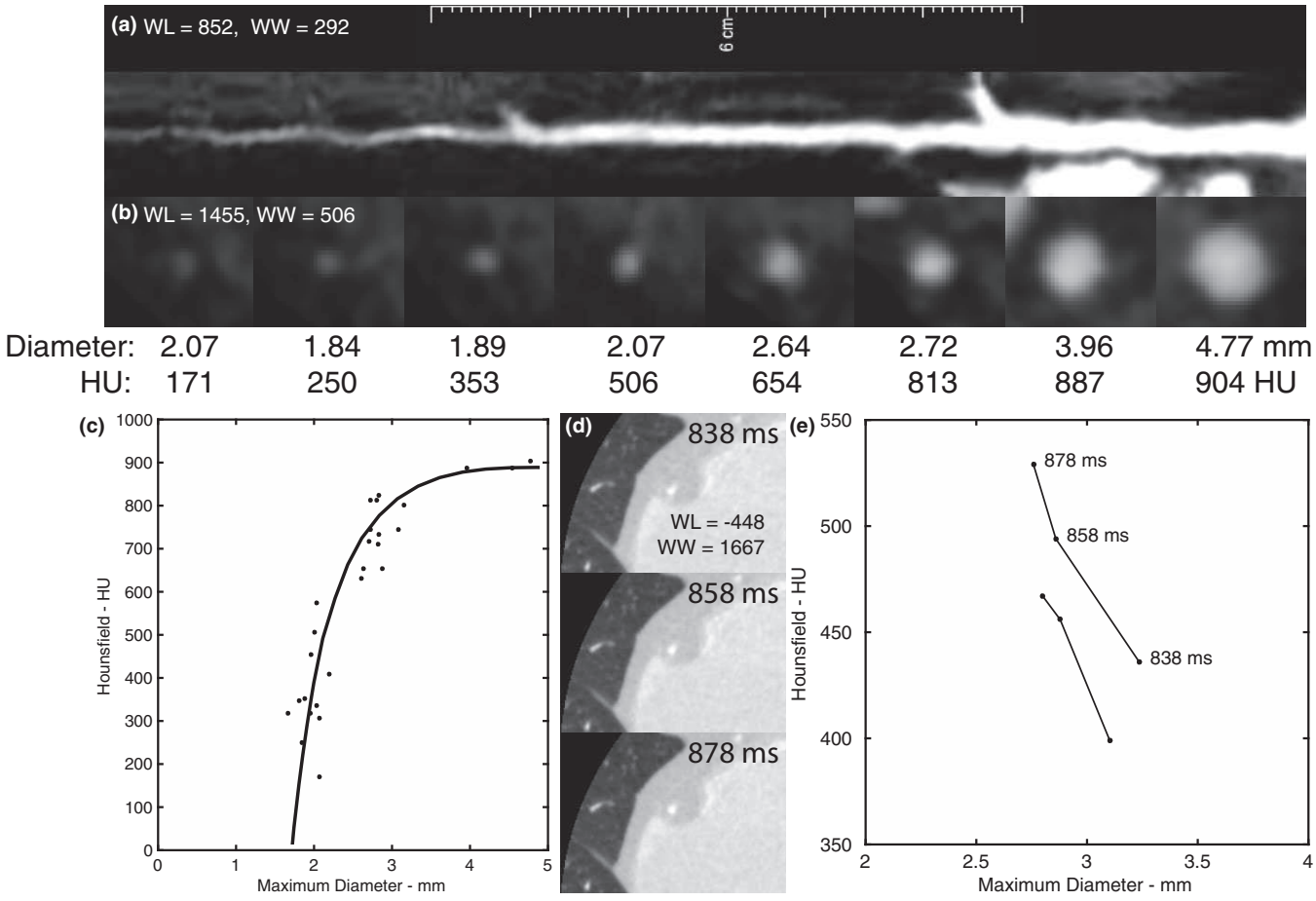

FIG. 1. Observed changes in vessel intensity and diameter on clinical CT scanning. (a) and (b) After centerline detection of the left anterior descending vessel, the intensity and diameter can be quantitated from cross-sectional images (c) The relationship between vessel intensity and diameter demonstrates two different imaging regimes. (d) and (e) The impact of small coronary vessel drift can be observed from reconstruction of three images of the right coronary artery approaching end-diastole. The vessel has a higher intensity and smaller diameter at later time points (878 ms). This was observed at two different slice positions.

anterior descending coronary vessel after centerline detection (qAngio, Medis Medical Imaging Systems, Leiden, Netherlands) are shown. Moving distally, the full width half maximum (FWHM) diameter of the vessel decreases until it reaches a limit (~2 mm) while the maximum vessel intensity decreases from 904 to 171 Hu. The relationship is plotted in Fig. 1(c). This plot illustrates two different imaging regimes: (a) vessels with diameters > 3 mm have near constant maximum vessel intensity but vary in diameter, (b) smaller vessels have varying maximum intensity (800 to 150 Hu) but near constant measured diameter. The impact of small motion on clinical patients can also be evaluated using these measures [Figs. 1(d) and 1(e)]. Images reconstructed at three time points (838, 858, and 878 ms after QRS detection) show an increase in intensity and decrease in diameter in a right coronary artery. This can be attributed to changes in amount of vessel motion in the reconstruction with more stationary vessels in the later time frames.

This paper explores the effect of two technical issues on estimating lesion geometry: (a) intrinsic scanner resolution as defined by the detector array and scanner geometry, and (b) small motions during data acquisition. First, we quantitate the decrease in signal intensity and increase in measured diameter associated with a reduction in true lumen diameter in static vessels. We then explore the effect of *small* drifts of the vessels during acquisition for commonly used reconstruction parameters. In both cases, the task we are focused upon is the quantitative characterization of vessel and lesion geometry under "best-case" imaging conditions (ideal spot size, noiseless data acquisition, sampling at the isocenter).

The results in this paper illustrate: (a) the limitations of measuring moderate and severe stenoses with clinical scanners and (b) the sensitivity of vessel caliber and intensity to small motions.

2. MATERIALS AND METHODS

In this simulation study, we developed a digital phantom, simulated projection data for a range of motions and vessel sizes, reconstructed full and half-scan datasets, and measured vessel parameters in images in which the vessels are stationary and those in which they undergo small motions at constant velocity. Motion and motion correction were applied by incorporating the known motion direction and magnitude into the forward and backward projectors. This section outlines each process in this study.

2.A. Digital coronary phantom design

A 3D coronary vessel phantom was computer generated with seven identical cylindrical coronary vessels, oriented in the z-dimension, at different radial positions (between 2.5 and 7 mm from the isocenter). Different phantoms with vessels ranging in diameter from 3.0 to 0.2 mm were generated which correspond to 0% to 93% stenosis of a 3.0 mm vessel (Fig. 2). The vessel phantom was generated with $0.025 \times 0.025 \times 0.5$ mm voxels; this oversampling by a factor of 16 in both x and y was used to calculate accurate projections for a standard clinical scanner detector geometry.

2.B. Coronary phantom motion

Coronary CTA is usually performed during diastasis, which occurs approximately 75% through the RR interval. During that time, for most patients, the coronary vessels are at their most quiescent[11]; however, because modern CTA image resolution is so high, even a small sub-millimeter drift of the vessel can modify the signal in the vessel. To introduce motion during data acquisition, a linear translation D_X was applied to each view such that a target total distance (TTD) was traversed in the horizontal direction over the course of $N_P = 800$ projections spanning 360° sampling of the object.

$$D_X(i) = TTD\frac{i}{N_p} \tag{1}$$

The range of motions simulated (TTD) was between 0 and 2.0 mm.

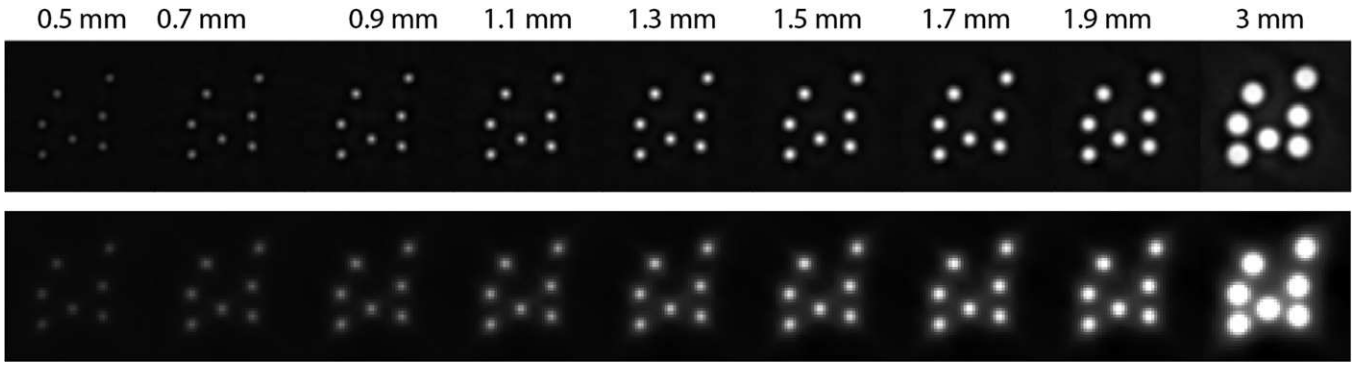

FIG. 2. Reconstructed images of computer generated stationary coronary vessels of different diameters used for quantitation of stenosis. For each diameter, seven vessels were placed at different radial distances from the isocenter. The degree of stenosis of a 3 mm vessel that these diameters represented were (%): 83, 77, 70, 63, 57, 50, 43, 37, and 0. Reconstructions were performed with 0.04×0.04 mm pixels (top row) for measurements of vessel characteristics. In addition, images with clinical resolution (0.4×0.4 mm pixels) demonstrate the effect of pixilation on vessels (bottom).

2.C. Sinogram simulation

For each time point t = 0: ($N_P - 1$), forward projections were acquired from the corresponding phantom volume. To investigate the effect of gantry position relative to the motion direction on motion sensitivity, five projections were acquired at each time step where i = 1:5 is the gantry position.

$$\phi(t,i) = 0.45°t + 22.5°(i - 1) \quad (2)$$

Sinograms were obtained via a ray-based forward projector modified for a curved detector geometry and implemented in Gadgetron (NIH, Bethesda, MD, USA) with 20-fold oversampling in the detector plane (u, v).[23–25] Oversampled sinograms were integrated to simulate the sampling achieved by a single-source Toshiba Aquilion ONE clinical scanner geometry (896 detectors per row, 320 detector rows with 0.5 mm effective detector length in the z-dimension at the isocenter, 1072 mm source-to-detector distance and 600 mm source-to-isocenter distance, quarter detector offset, and no flying focal spot)[26] using Matlab (Mathworks, Natick MA, USA). Although not a feature of the Toshiba Aquilion ONE scanner, we implemented in-plane focal spot deflection (FSD) to evaluate the potential improvement in performance for our task.[27] In this case, twice the number of volumes (and projections) were generated to account for the increase in acquired projections and the detector offset was modified from one-quarter to one-eight.

2.D. Image reconstruction

Both half-scan (180° plus fan) and full-scan (360°) reconstructions were performed using an iterative conjugate-gradient reconstruction (Gadgetron, NIH, Bethesda MD, USA).[23–25] Oversampled images (0.04 mm × 0.04 mm × 0.5 mm voxels, 200 × 200 × 20 mm field-of-view) as well as clinical-grade images (0.4 mm × 0.4 mm × 0.5 mm voxels, 200 × 200 × 20 mm field-of-view) were generated. Since the simulation was noiseless and we aimed to obtain the highest spatial resolution results, neither Tikhonov regularization, nor spatial regularization (e.g., total variation) nor non-negativity constraints were included. This also minimized the non-liner impacts of image reconstruction on measured vessel characteristics. Furthermore, the iterative approach does not require a ramp filter or kernel and results were obtained after either convergence or 20 iterations.

For comparison, reconstruction with a Feldkamp–Davies–Kress type reconstruction with both a Ram-Lak as well as a Hanning-like filter was performed. The Ram-Lak filter was used to increase spatial resolution while the Hanning-like filter is intended to reflect a clinical imaging scenario with a published filter that makes a good trade-off between the holding detail and suppressing noise.[28]

For both full and half-scan reconstructions, variations in the gantry position were performed as described in Eq. (2). The angular source position (SP) in the middle (M) of the acquisition was varied between parallel ($\theta_{SP,M} = 0°$) and orthogonal ($\theta_{SP,M} = 90°$) to the direction of phantom motion.

2.E. Coronary vessel measurements

The impact of vessel diameter, vessel motion, focal spot deflection, acquisition (half vs. full), reconstruction (iterative vs. FDK-type), and gantry position on coronary vessels was quantitated by measuring three vessel parameters: the signal intensity at the center, the vessel diameter, and ellipsoidal deformation.

The signal intensity was calculated as the average intensity within a 0.4 × 0.4 mm ROI at the center of each vessel. This region corresponds to the signal in the central pixel of a clinical-grade image.

To measure the vessel diameter and shape, the full width half maximum (FWHM) region of the vessel was identified using the signal intensity at the vessel center as the maximum. The diameter was calculated as the major axis of an ellipse fit to the full width half maximum contour. The shape of the ellipse was evaluated using the ratio of the major (a) and minor (b) axis = $\frac{a}{b}$.

The intensity, diameter, and major-to-minor axis ratio were calculated for each of the seven vessels at the central slice along the z-dimension and mean values are reported.

3. RESULTS

3.A. Measured characteristics of stationary vessels with full-scan reconstructions

For the scanner geometry used in this study, the attenuation measured in a stationary vessel decreased with decreasing vessel diameter [Fig. 3(a)] with a rapid drop in signal intensity for vessels smaller than 1.5 mm diameter. The measured diameter of the vessel closely resembled the true size for vessels between 1.5 and 3.0 mm; however, for vessels smaller than 1.5 mm, there is a noticeable overestimation of the true diameter [Fig. 3(b)]. Stationary vessels had major-to-minor axis ratios near 1 [Fig. 3(c)].

Figure 3(d) illustrates digital vessels and corresponding high-resolution images, FWHM contours, and clinical-resolution images. The high-resolution images illustrate the reduction in luminal intensity as the vessel diameter decreases while the FWHM contours demonstrate how the diameter of the vessel appears to reach a minimum value despite progressively decreasing true vessel size.

3.B. Impact of half-scan (180° plus fan angle) reconstruction on measured vessel characteristics

Relative to full-scan reconstruction, half-scans result in a decreased measured vessel intensity [Fig. 4(a)], increased vessel diameter [Fig. 4(b)], and increased vessel eccentricity [Fig. 4(c)], as a function of decreasing simulated vessel diameter, especially for vessels < 1.5 mm in diameter. For

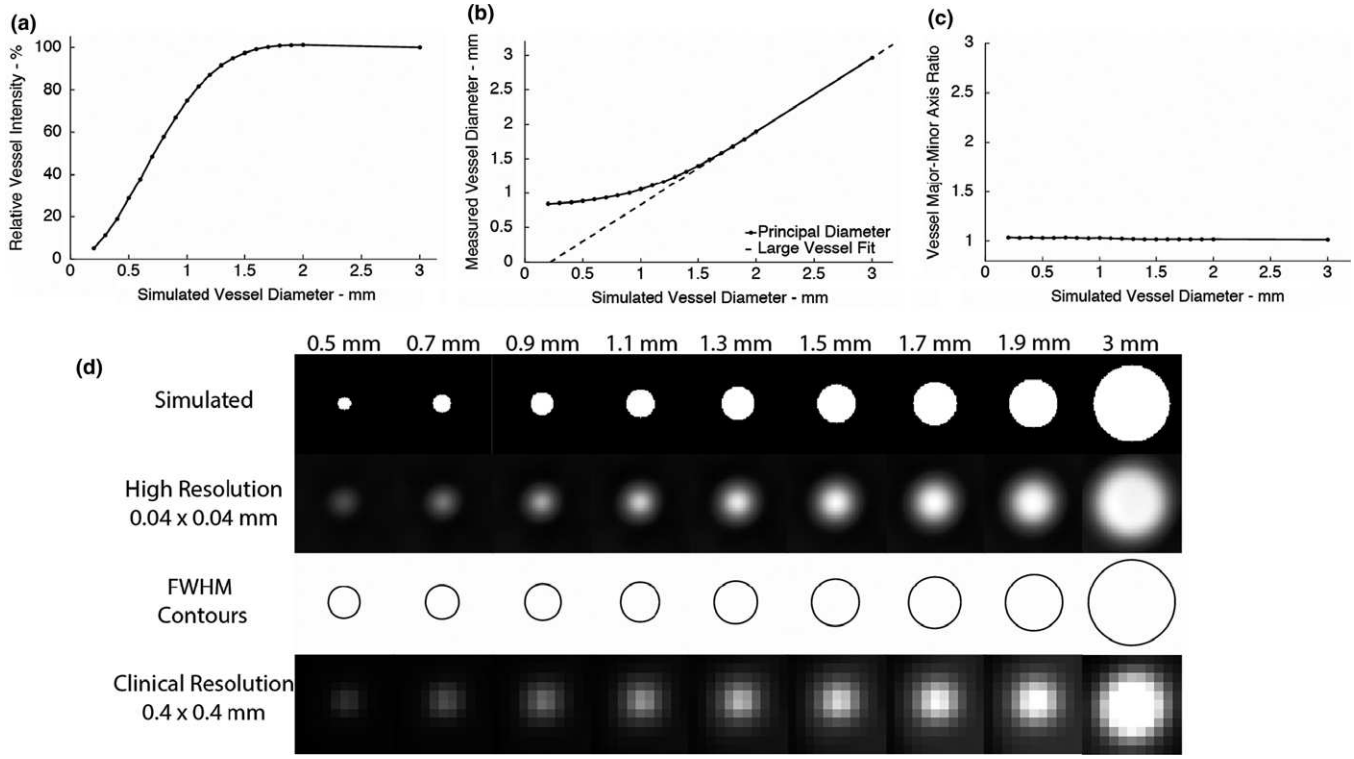

FIG. 3. Measured vessel characteristics of stationary vessels from full-scan reconstructions. (a) Measured vessel intensity as a function of simulated vessel diameter demonstrate the loss of intensity with decreasing vessel diameter. The points on the curve show data for each 0.1 mm reduction in simulated vessel diameter after 2.0 mm. (b) Measured vessel diameter as a function of the simulated vessel diameter. Vessels < 1.5 mm demonstrate a loss of diameter accuracy relative to accuracy observed in vessels between 1.7 and 3.0 mm (dotted line represents linear fit, $R^2 > 0.999$). (c) The shape of measured vessel was quantitated via the major-to-minor axis ratio as a function of simulated vessel diameter. Regardless of vessel diameter, there is close agreement between the major and minor vessel diameter. (d) Simulated and reconstructed vessel images and full width half maximum contours demonstrate the loss of intensity with decreasing vessel diameter and the error in measured diameter for vessels < 1.5 mm. Clinical-resolution reconstructions demonstrate the degree of pixelation associated with this vessel range.

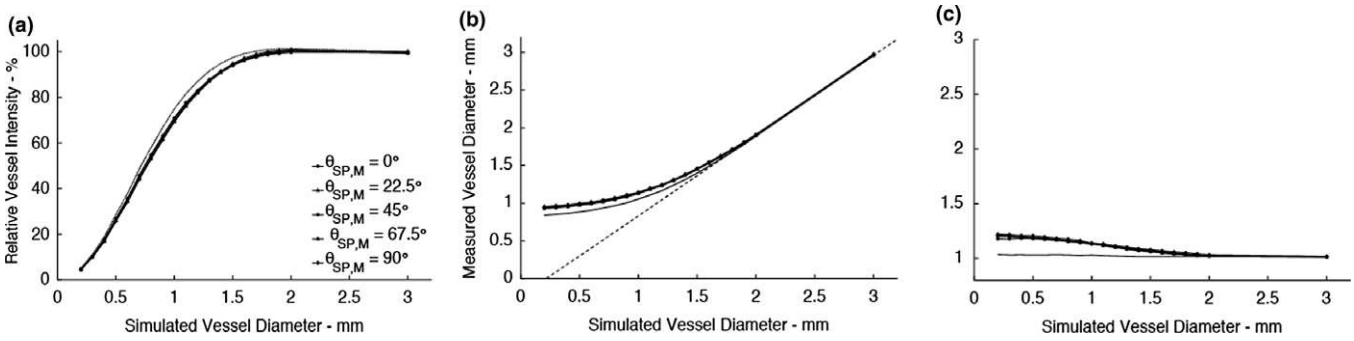

FIG. 4. Vessel characteristics of stationary vessels measured from half-scan reconstructions. Measured vessel intensity (a), vessel diameter (b), and vessel shape (c) demonstrate a small deviation from the full-scan results (solid black line).

stationary vessels, the position of the x-ray source in the middle of the half-scan did not result in noticeable differences in measured vessel characteristics.

3.C. Imaging Stationary vessels with quarter detector offset vs. in-plane focal spot deflection

Two approaches to increase sampling (quarter detector offset and in-plane focal spot deflection[27]) were implemented to evaluate the potential changes in performance. Figure 5(a) shows results of 0.2 mm diameter vessels imaged with half and full-scans with quarter detector offset (QDO) or with eight detector offset and focal spot deflection (FSD). For half-scans, focal spot deflection increases vessel intensity [Fig. 5(b)] and decreases in vessel diameter [Fig. 5(c)] relative to quarter detector results. An upwards and leftward shift of the intensity vs. diameter curve [Fig. 5(d)] can be observed for half-scans, suggesting a slight improvement in performance. For full-scans, the quarter detector offset yielded increased vessel intensity and decreased vessel diameter

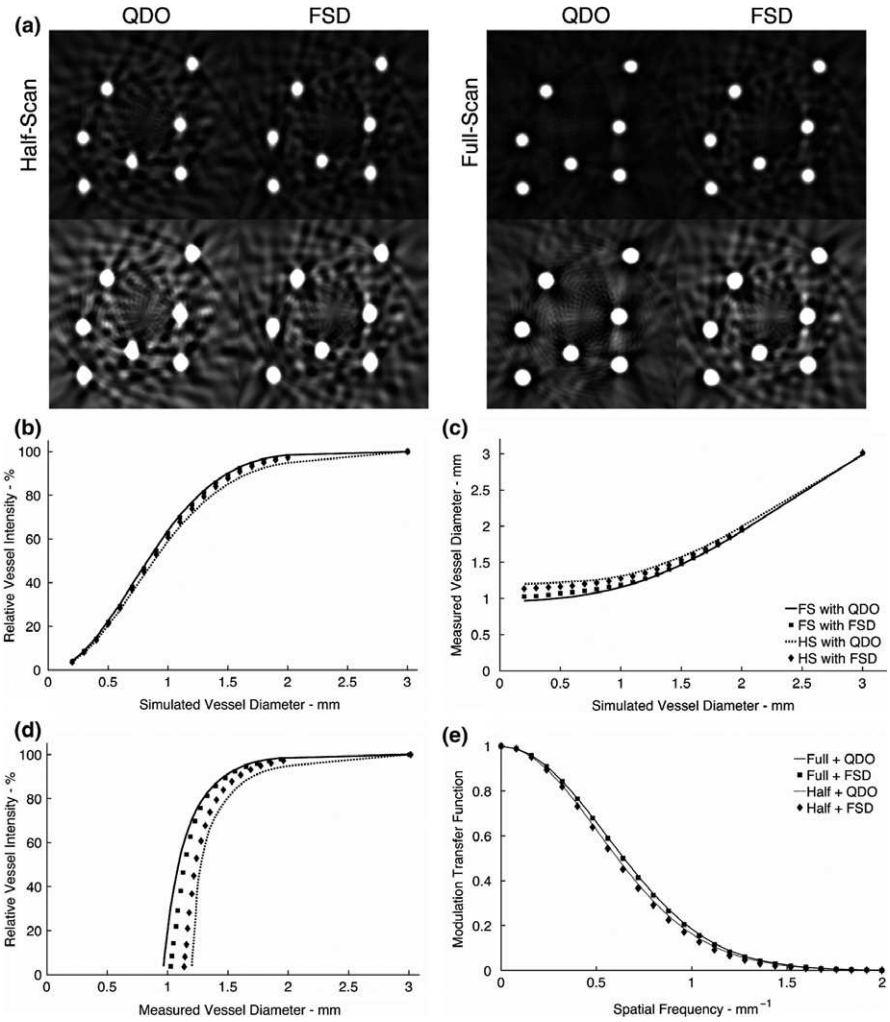

FIG. 5. Change in 0.2 mm diameter vessels and performance metrics with the use of quarter detector offset and focal spot deflection. (a) The effect of quarter offset deflection compared to focal spot deflection on full and half-scan reconstructions can be observed on the top row. For half-scans with focal spot deflection, there is (b) an increase in vessel intensity, (c) a decrease in measured vessel diameter, and (d) leftward-upward shift of the intensity-measure diameter curve suggesting an improvement in performance. For full-scans, the quarter detector offset results demonstrate improved performance over focal spot deflection (with one-eight detector offset). (e) Differences in MTF between the two approaches are small compared to differences between full and half-scanning.

resulting in an upwards and leftward shift of the intensity vs. diameter curve relative to focal spot deflection (with one-eight detector offset). Despite these differences in task-based measurements, the MTF of the two techniques are nearly identical [Fig. 5(e)].

3.D. Imaging stationary vessels with FDK-type reconstruction

To evaluate the impact of the reconstruction, images were reconstructed using both an iterative (filter-free) approach (solid line) as well as a FDK algorithm with a Hanning (dashed line) and Ram-Lak filter (diamond points). The vessel intensity, diameter, and eccentricity are shown in Figs. 6(a)–6(c). Figure 6(d) shows a rightward shift of the vessel intensity vs. measured diameter curve for the Hanning-filtered FDK. The images from 0.2 mm diameter vessels were used as PSF estimates to generate a two-dimensional MTF [Fig. 6(e)] with a cross-section show in Fig. 6(f).

3.E. Change in vessel measurements with small coronary motions in full-scans

Figures 7(a), 7(c), and 7(e) illustrate the loss of vessel intensity, increase in vessel diameter, and increase in the ellipsoidal nature of the vessel with a small vessel drift during acquisition. Each curve in Fig. 7(a) gives the result for a different level of motion for each vessel dimension. If we fix our attention at a specific true dimension on the x-axis, we can scan down vertically to see the relative reduction in intensity for each level of motion. For example, at a 1.5 mm diameter, a displacement of 1.8 mm causes the intensity to be 60% of the proximal vessel value (at 3.0 mm).

This additional reduction in intensity can make a 1.5 mm vessel (corresponding to a 50% stenosis of a 3 mm vessel) appear to have the intensity of a 0.8 mm stationary vessel (corresponding to a 75% stenosis). It is clear from these results that the intensity of vessels above 2.0 mm diameter are relatively unaffected by this small motion while smaller

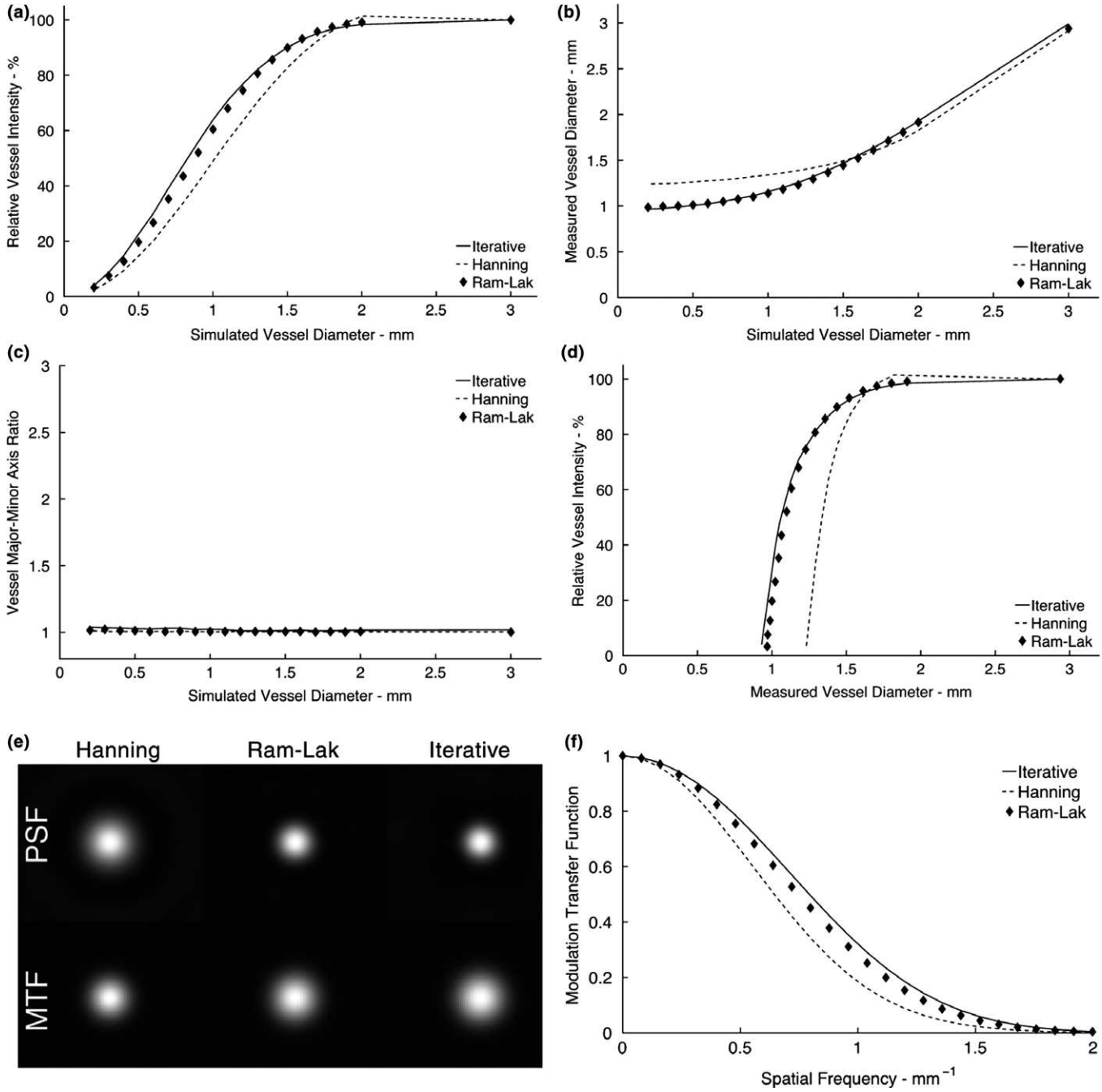

FIG. 6. Performance of iterative and FDK reconstructions. (a) Measured vessel intensity as a function of simulated vessel diameter demonstrate a loss of intensity for Hanning-filtered FDK in comparison to Ram-Lak FDK and iterative reconstructions. (b) Measured vessel diameter as a function of the simulated vessel diameter is comparable between Ram-Lak FDK and iterative but higher in Hanning-filtered FDK. (c) The shape of measured vessel was similar between all reconstructions. (d) The decrease in vessel intensity and increase in diameter results in a downward-rightward shift of the performance curve of the Hanning-filtered FDK in comparison to Ram-Lak and iterative results. (e) Images of 0.2 mm diameter vessels were used as PSF estimates to calculate the two-dimensional MTF. (f) The horizontal projection through the PSF highlights the difference in image resolution.

FIG. 7. Effect of small motion of vessels on the measured vessel characteristics. Measured vessel intensity (a), diameter (c), and shape (e) as a function of true vessel diameter for moving vessels with full reconstruction and without motion correction illustrate the loss of accuracy. The points along each curve give the result for different vessel diameters. The different labeled points show the result for different levels of constant motion as quantitated by the total displacement given in the legend in (c). Motion correction improves quantitation of vessel intensity (b), diameter (d), and shape (f). Vessel images (g) and FWHM contours (h) during 1.2 mm vessel translation during acquisition of full-scan data with and without correction highlight the loss of intensity and distortion of their circular shape as well as the recovery with motion correction.

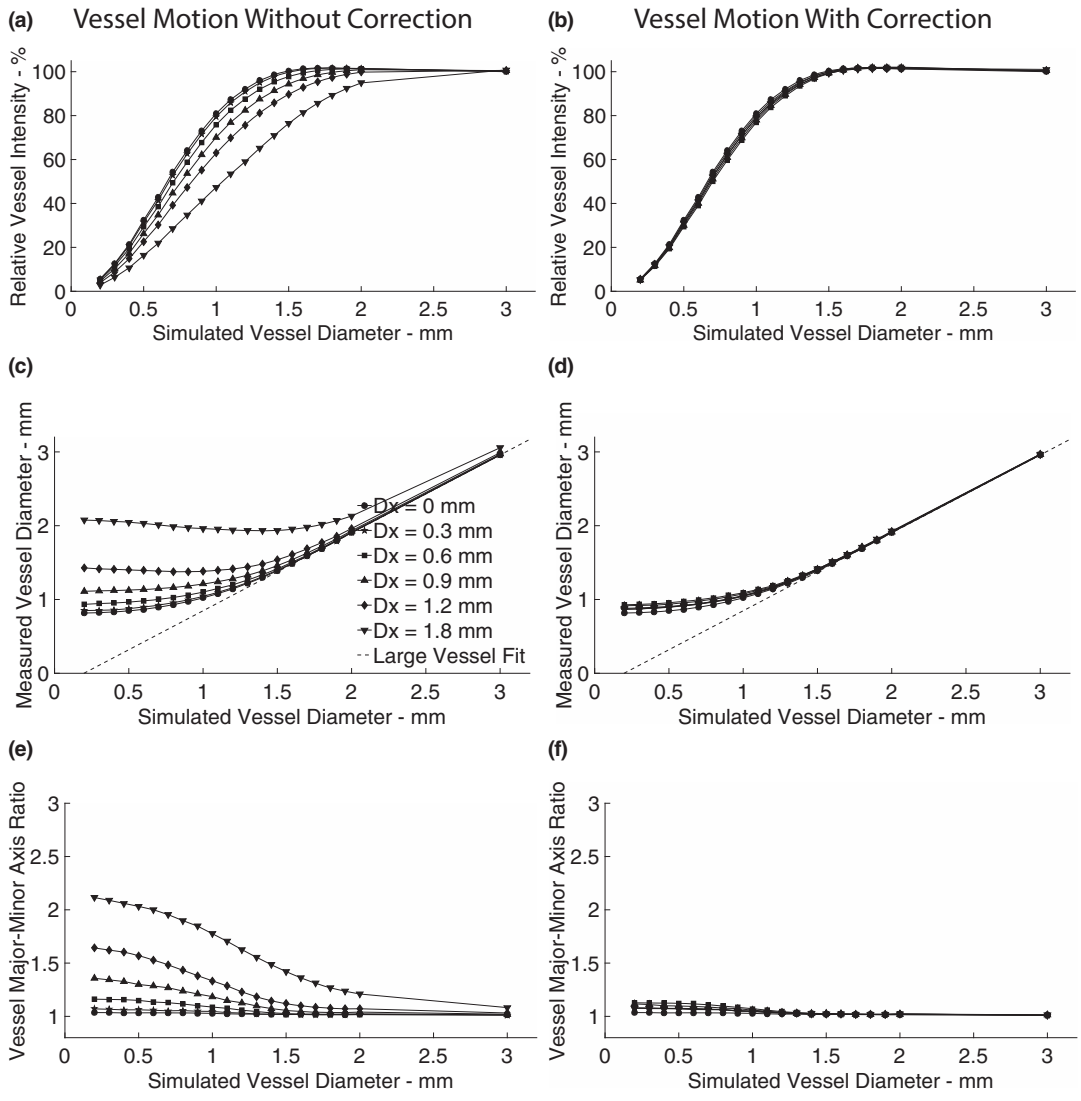
(a)
Vessel Motion Without Correction
Relative Vessel Intensity - %
Simulated Vessel Diameter - mm
(b)
Vessel Motion With Correction
Relative Vessel Intensity - %
Simulated Vessel Diameter - mm
(c)
Measured Vessel Diameter - mm
Dx = 0 mm
Dx = 0.3 mm
Dx = 0.6 mm
Dx = 0.9 mm
Dx = 1.2 mm
Dx = 1.8 mm
Large Vessel Fit
Simulated Vessel Diameter - mm
(d)
Measured Vessel Diameter - mm
Simulated Vessel Diameter - mm
(e)
Vessel Major-Minor Axis Ratio
Simulated Vessel Diameter - mm
(f)
Vessel Major-Minor Axis Ratio
Simulated Vessel Diameter - mm

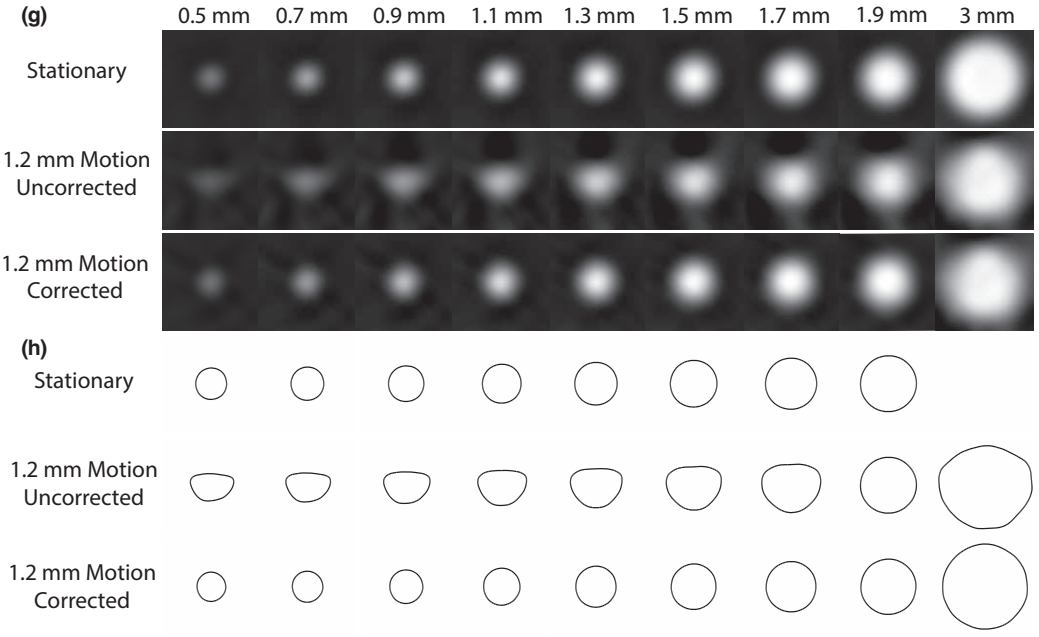
(g)
0.5 mm
0.7 mm
0.9 mm
1.1 mm
1.3 mm
1.5 mm
1.7 mm
1.9 mm
3 mm
Stationary
1.2 mm Motion Uncorrected
1.2 mm Motion Corrected
(h)
Stationary
1.2 mm Motion Uncorrected
1.2 mm Motion Corrected

vessels are more sensitive to motion. Figures 7(b), 7(d), and 7(f) demonstrate the improvement achieved via motion correction in the reconstruction algorithm. Unsurprisingly, correction of the displacement increases observed vessel intensity and improves estimation of vessel diameter and shape—essentially returning to the values measured in stationary vessels. Figures 7(g) and 7(h) illustrate the decrease in the vessel intensity and circularity due to an uncorrected 1.2 mm motion over 360° and how these values can be recovered with correct motion estimation.

3.F. Measured vessel intensity vs. diameter in full-scan reconstructions

The relationship between measured vessel intensity and measured vessel diameter in stationary and moving coronary vessels is shown in a single graph in Fig. 8(a). In stationary vessels, estimation of true vessel caliber for vessels smaller than ~1.5 mm becomes very difficult because all vessels smaller than 1.5 mm have approximately the same measured caliber (using FWHM as the quantitative estimate). It is also apparent that small motions of the vessels result in significant changes in both measured vessel diameter and intensity. Specifically, all vessels decrease their observed intensity and increase their observed caliber (downward-rightward shift of the curve).

Figure 8(b) demonstrates the improvement with motion correction. Incorporating motion of the vessels into the reconstruction recovers the relationship between vessel intensity and diameter seen in stationary vessels.

3.G. Impact of gantry position on full and half-scan reconstructions of moving coronary vessels

The impact of coronary vessel motion on both full and half-scan reconstructions depends on the position of the gantry with respect to the direction of vessel motion.[29] The velocity of the vessels was constant between half- and full-scan reconstruction. As a result, vessels imaged with a half-scans underwent less motion due to the decreased temporal duration of the acquisition. As can be seen in Figs. 9(a) and 9(b), the position of the gantry [central x-ray beam parallel to motion in (a) and orthogonal to motion in (b)] has an impact on the change in measured vessel intensity and diameter for full-scan acquisitions. In the parallel scenario [$\theta_{SP,M} = 0°$, Fig. 9(a)] the moving edges are sampled at two time points (25% and 75% of the scan). For the full-scan with the orthogonal scanning scenario [$\theta_{SP,M} = 90°$, Fig. 9(b)], the initial, middle and final portions of the scan sample the edges of the vessel in the motion direction; as a result, three different vessels positions are sampled.

The gantry position has a larger impact on the half-scan reconstructions. When the center of the acquisition is parallel to the direction of motion [$\theta_{SP,M} = 0°$, Fig. 9(c)], there is a considerable loss of accuracy because the first and last views of the vessel are at the extremes of the vessel locations during the motion and the projections used for reconstruction are sensitive to the displacement. If the center of the half-scan acquisition is orthogonal to the motion of the vessel [$\theta_{SP,M} = 90°$, Fig. 9(d)], motion has a minimal impact on quantitation of vessel intensity and diameter, and the location of the vessel is approximately at the center of the range of motion over the acquisition.

3.H. Clinical image reconstruction strategies in the presence of vessel motion and potential motion correction

We further explored the effect of four different imaging conditions, with and without motion correction: (a) full-scan reconstruction with $\theta_{SP,M} = 0°$, (b) full-scan reconstruction with $\theta_{SP,M} = 90°$, (c) half-scan reconstruction with $\theta_{SP,M} = 0°$, and (d) half-scan reconstruction with $\theta_{SP,M} = 90°$. Figures 10(a) and 10(b) demonstrate full-scans suffer the largest loss of performance due to uncorrected motion (open circles). However, motion correction of full-scans (solid points) results in performance which closely resembles imaging of stationary vessels with full-scans. For the half-scans, the impact of motion is less pronounced but there is a larger variation in the impact of motion and potential improvement with motion correction that is gantry dependent. When $\theta_{SP,M} = 0°$ [Fig. 10 (c)], motion results in

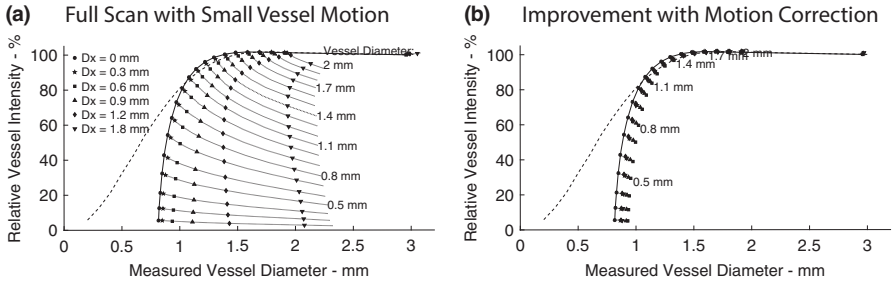

FIG. 8. Measured vessel intensity and diameter for moving vessels with full-scan reconstruction with and without motion correction. (a) Dashed line represents intensity vs. simulated vessel diameter relationship for stationary vessels described in Fig. 3(a). The measured intensity vs. measured diameter relationship is affected by uncorrected motion via a decrease in measured intensity and increase in measured diameter. (b) The use of motion correction during reconstruction improves measured vessel intensity and diameter.

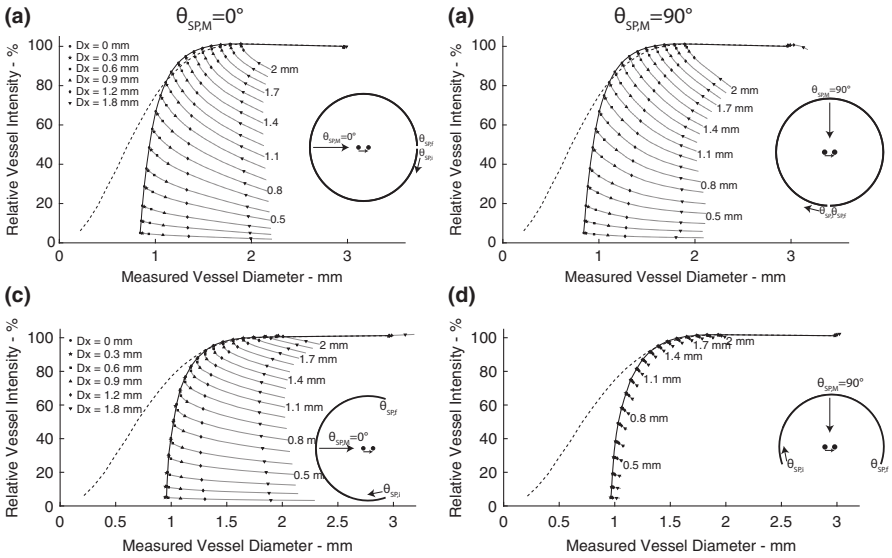

FIG. 9. Measured vessel intensity and diameter as a function of gantry position for full-scan (a) and (b) and half-scan (c and d) acquisitions. This figure shows source positions in the middle of the acquired data, $\theta_{SP,M} = 0°$ where this view is parallel to the motion (a) and (c), and $\theta_{SP,M} = 90°$, which is orthogonal to the direction of motion (b and d). (a) When $\theta_{SP,M} = 0°$, projections of the moving edge in the vessel are acquire at two time points. (b) When $\theta_{SP,M} = 90°$, the moving edge is sampled at the initial ($\theta_{SP,i}$), middle ($\theta_{SP,M}$), and final ($\theta_{SP,f}$) positions of the full-scan and result in three different spatial positions being sampled. This results in increased sensitivity to motion, particularly a larger decrease in intensity for a given motion. (c) Half scan acquisitions centered parallel to the motion; the moving edge is sampled at two time points ($\theta_{SP,i}$), and ($\theta_{SP,f}$) and, as a result, the measured vessel intensity decreases and diameter increases. (d) Half scan acquisitions with their center oriented orthogonal to the motion direction result in substantial motion insensitivity as the temporal window over which the moving edge is sampled is substantially reduced. *Note*: motion values Dx represent motion of the object over full (360°) scans. Therefore, the object will translate approximately half as far during the half-scan reconstruction.

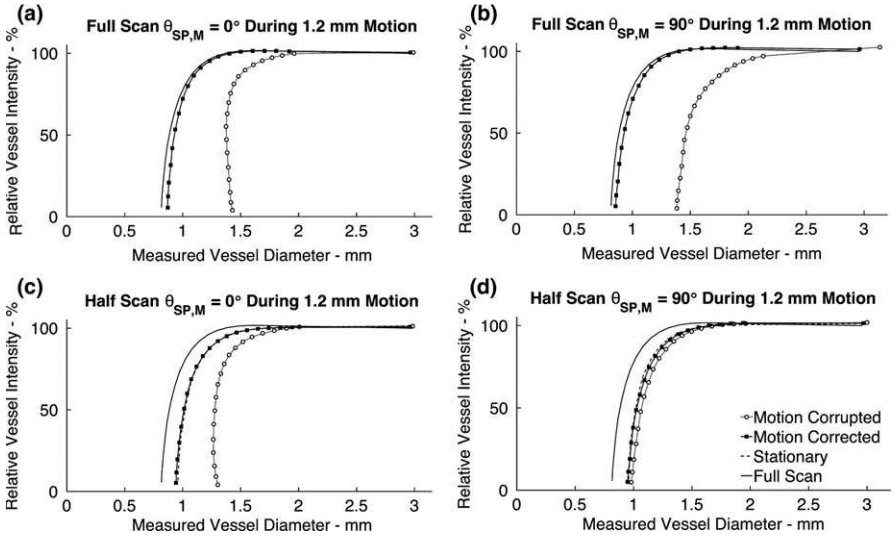

FIG. 10. Comparison of vessel intensity vs. measured diameter relationship for different imaging conditions. (a) and (b) The solid line in each graph gives the result from full scanning of stationary vessels. Full-scan images with uncorrected vessel motion (open circles) result in the largest decrease in vessel intensity and increase in vessel diameter. Use of motion correction results in measured vessel intensity and diameter that closely match measurements made during scans of stationary vessels. The dependence on gantry position can be seen in the subtle rightward and downward shift of the curve in the setting of motion corruption in (b) vs. (a). (c) Half-scan with $\theta_{SP,M} = 0°$ results in a substantial decrease in accuracy that can be partially recovered by motion correction. (c) Half-scan with $\theta_{SP,M} = 90°$ results in minimal change in measured vessel intensity or diameter with motion.

a *substantial* loss of performance which is recovered with motion correction. However, the loss of performance due to half-scanning persists. When $\theta_{SP,M} = 90°$ [Fig. 10(d)], motion results in *minimal* loss of performance; however, this result cannot be guaranteed clinically as the gantry position is not directly controlled and the motion direction of a vessel will vary as a function of position and cardiac cycle phase.

4. DISCUSSION

In this study, we have explored several elements critical to characterizing the geometry of coronary vessels and the estimated degree of stenosis. The results outline a series of key takeaways.

4.A. Scanner performance during full-scan reconstruction of stationary vessels

Figure 2 outlines the challenges faced by physicians when trying to grade a stenosis as mild, moderate, or severe. We found that for current clinical CT scanners, vessels with diameters <~1 mm will result in intensity values < 80% of the intensity at the center of the proximal segment. Therefore, measuring the diameter of a vessel using a contour derived from an intensity threshold will not yield accurate quantitation for lesions in the moderate and severe category. Furthermore, Fig. 2(b) outlines how a FWHM measurement can result in overestimation of diameter for vessels < 1.5 mm. These results are comparable to those found by Kline et al. in benchtop high-resolution computed tomography.[30] Application of this FWHM method could result in severe lesions being graded as moderate. Perhaps due to these issues, society guidelines do *not* outline quantitative approaches for vessel grading.[8,9] Specifically, "visual grading of coronary segment narrowing by ranges of stenosis is the current standard of practice and has been shown to provide useful clinical information relative to invasive coronary angiography".[8]

In the case modeled in this paper, a vessel caliber smaller than ~1 mm will not be measured via a FWHM operator, regardless of the true vessel diameter. This leads to a progressively larger overestimation of vessel diameter with decreasing true vessel diameter. However, as the vessel caliber decreases the measured intensity decreases rapidly; measuring this drop in intensity could be used to estimate the true vessel diameter.

An example will be illustrative of the problem we face. For a 3 mm vessel the diameters of three classes of lesion are: "mild" (3.0–1.5 mm), "moderate" (1.5–0.75 mm) and "severe" (0.75–0 mm). Hence, an essential task is to determine if a vessel is below 0.75 mm in diameter; however, from Fig. 2(a) it is clear that the *measured* diameter of a stationary vessel will not fall below ~1 mm; this means that we must use the concomitant drop in vessel intensity to estimate the lesion severity. For a stationary 0.75 mm vessel, the expected signal intensity within the measured 1 mm lumen will be ~50% of the signal intensity found in the 3 mm proximal portion of the vessel. In practice clinicians use this drop in signal intensity to "visually" estimate lesion severity and their accuracy is improved through experience.

4.B. Vessel intensity and measured diameter in stationary and moving vessels

As shown in Fig. 4(a), a small amount of uncorrected motion during the acquisition (say 1.2 mm over a full rotation) will cause an additional reduction in the vessel intensity and increase in the vessel width, which may result in misclassification of lesions. For example, for a 3 mm vessel, from Fig. 4(a) we can see that a stationary 1.5 mm diameter stenosis will have an intensity of ~95% of the proximal vessel intensity with a diameter close to the limit of the scanner resolution; this stenosis would be characterized as "mild". However, if the 1.5 mm stenosis moves 1.8 mm during the acquisition, the intensity value will decrease to ~50% of the proximal value and the diameter will increase to ~1.5 mm. If we grade the vessel in this case based on intensity, we may incorrectly attribute the decrease in signal to a vessel with a smaller caliber (~0.8 mm diameter) and overcall the degree of a stenosis as "severe".

Furthermore, the fractional changes in intensity and diameter are different between vessels of different sizes. As a result, measurements made in larger vessels are unfortunately relatively insensitive to small motions and may not be useful in detecting motion corruption in neighboring smaller vessels. This presents a significant problem for motion estimation algorithms attempting to measure these small motions.

We believe the method of displaying the relationship between measured intensity and vessel diameter for moving vessels is unappreciated by the clinical cardiology community and an understanding of this relationship is an important element of accurately estimating the true degree of stenosis. Also, understanding the effects of small motions on the signal intensity is essential. For clarity, the results in this paper demonstrate these relationships in the simplest scenarios: namely, noiseless data, constant motion, and an ideal spot size. These results should be expanded in future studies with more realistic scenarios.

4.C. Use of half-scan reconstructions

The use of half-scan reconstructions can possibly improve moving vessel intensity and diameter quantitation when compared to full-scans in the absence of motion correction. However, as initially shown by Maaß et al.[29] we have also demonstrated that this improvement is highly dependent on the angular position of the gantry with respect to the direction of motion. As demonstrated in Fig. 4(a), if the start and end views of a half-scan are in directions perpendicular to the motion of the vessel, these views will sample the vessel at extreme positions and a large artifact will result. During clinical acquisition of data, the gantry continually rotates and data is acquired when the correct cardiac phase is identified on an ECG signal. As a result, the spatial position of the gantry at the start of data acquisition for a half-scan reconstruction at a certain cardiac phase is not controlled. In addition, the direction of motion will not be the same for different positions in the coronary vessel tree. Therefore, for a certain amount of coronary vessel motion, some half-scan acquisitions may deliver near-optimal results while others may lead to degradation comparable to a full-scan acquisition.

4.D. Clinical application of results

In addition to characterization of vessel caliber, CCTA can be used to assess whether a plaque is calcified or non-calcified. However, identifying features of vulnerable lesions based on lipid deposition or the presence of a thin fibrous cap has proven challenging.[31,32] The findings we present on small caliber vessel geometry can also be applied to plaque characterization. Specifically, plaque features are likely affected by motion in a similar fashion to the vessel lumen. For example, motion of a 0.5 mm diameter calcified plaque will likely result in a dimmer, larger, and eccentric feature while the larger, adjacent lumen may not demonstrate considerable motion corruption. This artifact from a small motion could be the source of additional calcium "blooming" artifact in addition to the natural dispersion of the high calcium signal by the system point spread function.

Our results present potential limitations of techniques used to estimate vessel motion. Specifically, large vessels (2–3 mm diameter) demonstrated a relative insensitivity to small motions. This corroborates the clinical experience of routine accurate assessment of patency of these vessels in the absence of large motions. Unfortunately, for this reason, these larger vessels may not be useful in detecting and estimating the small motions which can impact the measured characteristics of smaller vessels or stenoses.

4.E. Study limitations

This study has several limitations. First, the simulations were performed to assess performance in a "best-case" image scenario (a) with an infinitesimally small spot size (b) in the absence of noise and (c) near the isocenter. The lack of noise allowed reconstructions designed to maximize the spatial resolution (unregularized iterative reconstruction and Ram-Lak filtered FDK) while the isocenter position minimized sampling artifacts and reduced the impact of blurring due to continuous gantry and source motions. As a result, further simulation studies which capture the more realistic elements of clinical imaging and experiments with physical phantoms are planned to investigate each of these factors.

We intentionally used a kernel-free reconstruction and high-resolution pixel grid to attempt to isolate the effects of the intrinsic resolution of clinical gantry design on coronary quantitation. However, in clinical scanning, there is a necessary trade-off between the achievable spatial resolution and noise characteristics of the reconstructed images which we expect will reduce the performance (as demonstrated by the results of the FDK reconstruction with Hanning filter).

Our goal was to evaluate performance for a scanner with detector resolution, magnification, and gantry rotation velocity of clinical scans. These results could be generalized to any detector geometry but we expect shifts in the spatial position of the measured vessel intensity and measured vessel diameter curves. Although we included results comparing quarter detector offset and in-plane focal spot deflection, we believe this framework could be used to evaluate the quantitative impact of different filter designs, novel reconstruction techniques, and scanner designs (impact of spot size, detector size).

We limited our study to a single-source scanner design. Dual-source designs decrease the time required for data acquisition which would decrease the extent of motion observed. However, two sources may lead to discontinuities in the acquired sinogram during motion as the vessel position will change between the last projection acquired with the first source and the first projection acquired with the second source. Investigation of the effects of small motions on dual-source geometries deserves an independent study.

The process of *estimating* vessel motion was not included in the simulation. Several recent publications have presented methods, which we believe can be utilized to obtain an estimate of the vessel motion.[33,34] Our results outline the loss and potential recovery of performance in the setting of ideal motion estimation, while accurately representing the constraints of the clinical detector geometry.

Finally, this manuscript focused on constant velocity motions. Although the coronaries will accelerate during different periods of the cardiac cycle, we believe the motion in a small temporal window (~275 ms) can be approximated as a constant velocity for many patients. We chose this simplest motion model as a first order mapping of the magnitude of the effect of small motions. Studies evaluating imaging performance for non-linear motion models are planned as future work.

ACKNOWLEDGMENTS

This work was supported by the National Institutes of Health (grant number K12GM068524), University of California President's Postdoctoral Fellowship, and UC San Diego Frontiers of Innovation Scholar Program.

CONFLICTS OF INTEREST

The authors have no relevant conflicts of interest to disclose.

[a)]Author to whom correspondence should be addressed. Electronic mail: fcontijoch@ucsd.edu.

REFERENCES

1. Budoff MJ, Dowe D, Jollis JG, et al. Diagnostic performance of 64-multidetector row coronary computed tomographic angiography for evaluation of coronary artery stenosis in individuals without known coronary artery disease: results from the prospective multicenter ACCURACY (Assessment by Coronary Computed Tomographic Angiography of Individuals Undergoing Invasive Coronary Angiography) trial. *J Am Coll Cardiol*. 2008;52:1724–1732.
2. Chen MY, Bandettini WP, Shanbhag SM, et al. Concordance and diagnostic accuracy of vasodilator stress cardiac MRI and 320-detector row coronary CTA. *Int J Cardiovasc Imaging*. 2014;30:109–119.

3. Williams MC, Hunter A, Shah ASV, et al. Use of coronary computed tomographic angiography to guide management of patients with coronary disease. *J Am Coll Cardiol*. 2016;67:1759–1768.
4. Litt HI, Gatsonis C, Snyder B, et al. CT angiography for safe discharge of patients with possible acute coronary syndromes. *N Engl J Med*. 2012;366:1393–1403.
5. Hoffmann U, Truong QA, Schoenfeld DA, et al. Coronary CT angiography versus standard evaluation in acute chest pain. *N Engl J Med*. 2012;367:299–308.
6. Yeboah J, McClelland RL, Polonsky TS, et al. Comparison of novel risk markers for improvement in cardiovascular risk assessment in intermediate-risk individuals. *JAMA*. 2012;308:788.
7. Douglas PS, Hoffmann U, Patel MR, et al. Outcomes of anatomical versus functional testing for coronary artery disease. *N Engl J Med*. 2015;372:1291–1300.
8. Mark DB, Berman DS, Budoff MJ, et al. ACCF/ACR/AHA/NASCI/SAIP/SCAI/SCCT 2010 expert consensus document on coronary computed tomographic angiography. A report of the american college of cardiology foundation task force on expert consensus documents. *J Am Coll Cardiol*. 2010;55:2663–2699.
9. ACR–NASCI–SPR. Practice parameter for the performance and interpretation of cardiac Computed Tomography (CT), Resolution 39; 2014.
10. Shechter G, Resar JR, McVeigh ER. Displacement and velocity of the coronary arteries: cardiac and respiratory motion. *IEEE Trans Med Imaging*. 2006;25:369–375.
11. Husmann L, Leschka S, Desbiolles L, et al. Coronary artery motion and cardiac phases: dependency on heart rate – implications for CT image reconstruction. *Radiology*. 2007;245:567–576.
12. De Bruyne B, Fearon WF, Pijls NHJ, et al. Fractional flow reserve-guided PCI for stable coronary artery disease. *N Engl J Med*. 2014;371:1208–1217.
13. Douglas PS, Pontone G, Hlatky MA, et al. Clinical outcomes of fractional flow reserve by computed tomographic angiography-guided diagnostic strategies vs. usual care in patients with suspected coronary artery disease: the prospective longitudinal trial of FFRct: outcome and resource impacts stud. *Eur Heart J*. 2015;36:3359–3367.
14. Maurovich-Horvat P, Ferencik M, Voros S, Merkely B, Hoffmann U. Comprehensive plaque assessment by coronary CT angiography. *Nat Rev Cardiol*. 2014;11:390–402.
15. Sankaran S, Kim HJ, Choi G, Taylor CA. Uncertainty quantification in coronary blood flow simulations: impact of geometry, boundary conditions and blood viscosity. *J Biomech*. 2016;49:2540–2547.
16. Meinel FG, Canstein C, Schoepf UJ, et al. Image quality and radiation dose of low tube voltage 3rd generation dual-source coronary CT angiography in obese patients: a phantom study. *Eur Radiol*. 2014;24:1643–1650.
17. Dewey M, Zimmermann E, Deissenrieder F, et al. Noninvasive coronary angiography by 320-row computed tomography with lower radiation exposure and maintained diagnostic accuracy: comparison of results with cardiac catheterization in a head-to-head pilot investigation. *Circulation*. 2009;120:867–875.
18. Achenbach S, Ropers D, Kuettner A, et al. Contrast-enhanced coronary artery visualization by dual-source computed tomography—initial experience. *Eur J Radiol*. 2006;57:331–335.
19. Chen MY, Shanbhag SM, Arai AE. Submillisievert median radiation dose for coronary angiography with a second-generation 320-detector row CT scanner in 107 consecutive patients. *Radiology*. 2013;267:76–85.
20. Leipsic J, Labounty TM, Hague CJ, et al. Effect of a novel vendor-specific motion-correction algorithm on image quality and diagnostic accuracy in persons undergoing coronary CT angiography without rate-control medications. *J Cardiovasc Comput Tomogr*. 2012;6:164–171.
21. Fuchs TA, Stehli J, Dougoud S, et al. Impact of a new motion-correction algorithm on image quality of low-dose coronary CT angiography in patients with insufficient heart rate control. *Acad Radiol*. 2014;21:312–317.
22. Nett BE, Pack JD, Okerlund D, "Task based assessment of a motion compensation algorithm via simulation of a moving stenotic vessel," 8668, 86682B; 2013.
23. Hansen MS, Sorensen TS, Sørensen TS. Gadgetron: an open source framework for medical image reconstruction. *Magn Reson Med*. 2013;69:1768–1776.
24. Christoffersen CPV, Hansen D, Poulsen P, Sorensen TS. Registration-based reconstruction of four-dimensional cone beam computed tomography. *IEEE Trans Med Imaging*. 2013;32:2064–2077.
25. Zeng GL, Gullberg GT. Unmatched projector/backprojector pairs in an iterative reconstruction algorithm. *IEEE Trans Med Imaging*. 2000;19:548–555.
26. Centre for Evidence-based Purchasing (CEP). NHS Purchasing and Supply Agency. Comparative specifications 128 to 320 slice CT scanners technical specifications; 2009.
27. Kachelrieß M, Knaup M, Penßel C, Kalender WA. Flying focal spot (FFS) in cone-beam CT. *IEEE Trans Nucl Sci*. 2006;53:1238–1247.
28. Guo J, Zeng L, Zou X. An improved half-covered helical cone-beam CT reconstruction algorithm based on localized reconstruction filter. *J Xray Sci Technol*. 2011;19:293–312.
29. Maaß C, Kachelrieß M. Quantification of temporal resolution and its reliability in the context of TRI – PICCS and dual source CT. *Proc SPIE*. 2011;7961:1–7.
30. Kline TL, Zamir M, Ritman EL. Accuracy of microvascular measurements obtained from micro-CT images. *Ann Biomed Eng*. 2010;38:2851–2864.
31. Obaid DR, Calvert PA, Gopalan D, et al. Atherosclerotic plaque composition and classification identified by coronary computed tomography: assessment of computed tomography-generated plaque maps compared with virtual histology intravascular ultrasound and histology. *Circ Cardiovasc Imaging*. 2013;6:655–664.
32. Nakazato R, Otake H, Konishi A, et al. Atherosclerotic plaque characterization by CT angiography for identification of high-risk coronary artery lesions: a comparison to optical coherence tomography. *Eur Hear J Cardiovasc Imaging*. 2014;16:373–379.
33. Kim S, Chang Y, Ra JB. Cardiac motion correction based on partial angle reconstructed images in x-ray CT. *Med Phys*. 2015;42:2560–2571.
34. Sisniega A, Stayman JW, Cao Q, Yorkston J, Siewerdsen JH, Zbijewski W. Image-based motion compensation for high-resolution extremities cone-beam CT. *Proc SPIE Int Soc Opt Eng*. 2016;9783:97830K.